



ELSEVIER

Contents lists available at ScienceDirect

Mechanical Systems and Signal Processing

journal homepage: www.elsevier.com/locate/ymssp



Bayesian spectral density approach for identification of bridge section's flutter derivatives operated in turbulent flow

Xiaolei Chu ^a, Wei Cui ^{a,b,*}, Peng Liu ^a, Lin Zhao ^{a,b,c}, Yaojun Ge ^{a,b}

^a State Key Lab of Disaster Reduction in Civil Engineering, Tongji University, Shanghai, 200092, China

^b Key Laboratory of Transport Industry of Bridge Wind Resistance Technologies, Tongji University, Shanghai, 200092, China

^c State Key Laboratory of Mountain Bridge and Tunnel Engineering, Chongqing Jiaotong University, Chongqing, 400074, China

ARTICLE INFO

Communicated by S. De Rosa

Keywords:

Bayesian spectral density approach
Flutter derivatives
Complex Wishart distribution
Wind tunnel test
Bayesian inference
Markov chain Monte-Carlo sampling

ABSTRACT

This study presents a Bayesian spectral density approach for identification of flutter derivatives of bridge sections utilizing buffeting displacement responses, where the wind tunnel test is conducted in turbulent flow. Different from traditional time-domain approaches (e.g., least square method and stochastic subspace identification), the newly-proposed approach is operated in frequency domain. Based on the affine invariant ensemble sampler algorithm, Markov chain Monte-Carlo sampling is employed to accomplish the Bayesian inference. The probability density function of flutter derivatives is modeled based on complex Wishart distribution, where probability serves as the measure. By the Bayesian spectral density approach, the most probable values and corresponding posterior distributions (determined by conditions of measured signals) of each flutter derivative can be obtained at the same time. Firstly, numerical simulations are conducted and the identified results are accurate. Secondly, thin plate model, flutter derivatives of which have theoretical solutions, is chosen to be tested in turbulent flow for the sake of verification. The identified results of thin plate model are consistent with the theoretical solutions. Thirdly, the center-slotted girder model, which is widely-utilized long-span bridge sections in current engineering practice, is employed to investigate the applicability of the proposed approach on a general bridge section. For the center-slotted girder model, the flutter derivatives are also extracted by least square method in uniform flow to cross validate the newly-proposed approach. The identified results by two different approaches are compatible.

1. Introduction

Flutter derivatives (FDs) are of vital importance for long-span bridges, which are employed to estimate the flutter critical wind speed [1,2] and buffeting responses [3]. Conventionally, there are two popular identification schemes to extract FDs in the wind tunnel test. The first one is achieved by a forced vibration test, where the bridge sectional model is assumed to be rigid and supported by a machine (which can move as the predefined displacement's time series) [4,5]. The second one is by free vibration test, where the bridge sectional model is suspended by springs to move in vertical, torsional, and even lateral directions [6,7]. Two schemes mentioned above are both time-domain methods.

As for the forced vibration test, FDs are determined by moving the bridge sectional model in a predefined motion and the aerodynamic forces are being measured at the same time [8,9]. Usually, forced vibration tests, involved with sinusoidal vertical, torsional, and horizontal motions, are conducted for designs of bridges [10]. Recently, Zhao et al. [11] and Siedziako et al. [12]

* Correspondence to: 320 Wind Engineering Building, Tongji University, 1239 Siping Road, Shanghai, 200092, China.

E-mail address: cuiwei@tongji.edu.cn (W. Cui).

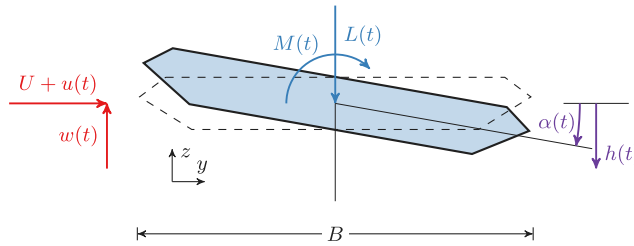


Fig. 1. Bridge section and coordinate definition.

developed the new equipments, which can simultaneously make the bridge sectional model move randomly in vertical, torsional, and lateral directions. As for the free vibration test, there are lots of identification methodologies developed to extract FDs in uniform flow, such as the unifying least-squares method [13,14] and iterative least-squares method [15]. Several researchers also identify the lateral-motion related FDs [16,17]. Furthermore, some stochastic identification methodologies are developed to extract FDs by utilizing buffeting displacement responses. Qin and Gu [18,19], Janesupasaeree and Boonyapinyo [20], and Mishra et al. [21] developed the covariance-driven stochastic subspace identification algorithm (SSI) to extract FDs in turbulent flow. Boonyapinyo and Janesupasaeree [22] also developed the data-driven SSI algorithm to extract FDs in turbulent flow. Recently, Wu et al. [23] utilized the unscented Kalman filter approach for identification of linear and nonlinear FDs of bridge decks, which can be operated either by free vibration or by buffeting response. However, all methodologies listed above are operated in time domain. Identification of FDs in frequency domain is rarely explored. Furthermore, substantial emphasis has been laid on FDs' experimental uncertainty (i.e., conduct the experiments under the same preset condition many times to get a set of different identified FDs, then get the probability density function of FDs) [24,25]. But the identification uncertainty, caused by the condition of measured signals (such as the sampling duration [26]), is also rarely discussed. As a result, the purpose of this study is to establish a probabilistic model to analyze the probability density functions (PDFs) of FDs. It should be stressed that the turbulence produced in a wind tunnel usually has a small integral scale compared to the model length, which may compromise the accuracy of the identified results. This problem is faced by all researchers who utilized the buffeting displacement responses [18,20,22,23]. But since what people used were not distributed parameters (e.g., wind pressure [27]), they only used buffeting forces acting on the whole section model. As a result, though such a deficiency exists, researchers can still get satisfactory results [18,20,22,23].

Except for SSI and Kalman filter, Bayesian system identification approach is another popular stochastic identification methodology for parameter inference of predefined mathematical models using input-output or output-only dynamic measurements, where probability serves as the measure [28]. Beck [28] detailedly illustrated the probability logic with Bayesian updating, providing a rigorous framework to quantify modeling uncertainty and to perform system identification [29]. Bayesian system identification has been successfully applied on the fields of structural modal identification [30–35], damage detection [36–39], and identification of soil stratification [40,41], etc. Besides, Yuen [42] employed the complex Wishart distribution [43] (namely Bayesian spectral density approach in [42]) to infer the most probable values (MPVs) and corresponding posterior uncertainty of structural parameters (modal frequencies, damping ratios, mode shapes) utilizing the power spectral density (PSD) of the random dynamic responses, which was a paradigm for parameter inference in a stochastic process. The identified quality depends on the accuracy of the predefined mathematical model [42]. Au [26] developed the fast Bayesian FFT algorithm, where the non-overlapping average is avoided compared with the Bayesian spectral density approach [42]. Au [44] also reveals the apparent mathematical equivalence between the Bayesian FFT method and the Bayesian spectral density approach. In [26], Au derived the theoretical c.o.v. (coefficient of variance) of each inferred parameter's posterior distribution in detail, and Au found that the c.o.v. was inversely proportional to the number of frequency points in the selected band. This conclusion means that if people want to decrease the posterior uncertainty, one efficient solution is to increase the frequency resolution (i.e., increase the sampling duration), which will lead to more frequency points included in the selected band. Typically, the posterior PDF of the inferred parameters \$\theta\$ can be well approximated by a Gaussian distribution \$G(\theta; \hat{\theta}, H(\hat{\theta})^{-1})\$ with mean value \$\hat{\theta}\$ and covariance matrix \$H(\hat{\theta})^{-1}\$ [42], where \$H(\hat{\theta})\$ denotes the Hessian matrix calculated at \$\hat{\theta}\$. A more efficient way is to use Markov chain Monte-Carlo (MCMC) sampling, which can obtain the posterior PDF directly [45–47]. In this paper, Bayesian spectral density approach [42] is employed to extract FDs in turbulent flow utilizing buffeting displacement responses, where the affine invariant ensemble sampler (AIES) MCMC [48,49] is used to obtain the posterior PDFs of FDs.

2. Bayesian spectral density formulation

2.1. Spectral density characteristics of bridge sectional model

In the wind tunnel test, a bridge sectional model with two degree-of-freedom (DOF), i.e., \$h\$ (vertical motion) and \$\alpha\$ (torsional motion), is often utilized, as shown in Fig. 1. The dynamic behavior of the sectional model in turbulent flow can be described by the following differential equations [50]:

$$m [\ddot{h}(t) + 2\xi_h \omega_h \dot{h}(t) + \omega_h^2 h(t)] = L_{se}(t) + L_b(t) \quad (1a)$$

$$I [\ddot{\alpha}(t) + 2\xi_\alpha \omega_\alpha \dot{\alpha}(t) + \omega_\alpha^2 \alpha(t)] = M_{se}(t) + M_b(t) \quad (1b)$$

where m and I are the mass and the mass moment of inertia of the deck per unit span, respectively; ω_i is the natural circular frequency, ξ_i is the damping ratio ($i = h, \alpha$); L_{se} and M_{se} are the self-excited lift and moment forces, respectively; L_b and M_b are the buffeting lift and moment forces due to turbulence with zero means.

The self-excited lift and moment forces are given as follows [3]:

$$L_{se} = \rho U^2 B \left[K_h H_1^*(K_h) \frac{\dot{h}}{U} + K_\alpha H_2^*(K_\alpha) \frac{B\dot{\alpha}}{U} + K_\alpha^2 H_3^*(K_\alpha) \alpha + K_h^2 H_4^*(K_h) \frac{h}{B} \right] \quad (2a)$$

$$M_{se} = \rho U^2 B^2 \left[K_h A_1^*(K_h) \frac{h}{U} + K_\alpha A_2^*(K_\alpha) \frac{B\dot{\alpha}}{U} + K_\alpha^2 A_3^*(K_\alpha) \alpha + K_h^2 A_4^*(K_h) \frac{h}{B} \right] \quad (2b)$$

where ρ is the air mass density; B is the width of the bridge deck; U is the mean wind speed at the bridge deck level; $K_i = \omega_i B/U$ is the reduced frequency ($i = h, \alpha$); H_i^* and A_i^* are the so-called flutter derivatives (FDs), which are usually considered to be related with reduced frequency and cross-sectional shape.

The buffeting lift and moment forces can be defined as [50]:

$$L_b(t) = \frac{1}{2} \rho U^2 B \left[2C_L \frac{u(t)}{U} \chi_L + (C'_L + C_D) \frac{w(t)}{U} \chi_L \right] \quad (3a)$$

$$M_b(t) = \frac{1}{2} \rho U^2 B^2 \left[2C_M \frac{u(t)}{U} \chi_M + (C'_M) \frac{w(t)}{U} \chi_M \right] \quad (3b)$$

where C_L , C_D , and C_M are the steady aerodynamic force coefficients; C'_L and C'_M are the derivatives of C_L and C_M with respect to the angle of attack, respectively; $u(t)$ and $w(t)$ are the longitudinal and vertical fluctuations of the wind speed, respectively, with zero means; χ_L and χ_M are the lift and moment aerodynamic admittances of the bridge deck, which are functions of frequency.

For the sake of brevity, denote the modified FDs as:

$$\begin{aligned} H_1 &= \frac{\rho B^2 \omega_h}{m} H_1^*(K_h), H_2 = \frac{\rho B^3 \omega_\alpha}{m} H_2^*(K_\alpha), H_3 = \frac{\rho B^3 \omega_\alpha^2}{m} H_3^*(K_\alpha), H_4 = \frac{\rho B^2 \omega_h^2}{m} H_4^*(K_h), \\ A_1 &= \frac{\rho B^3 \omega_h}{I} A_1^*(K_h), A_2 = \frac{\rho B^4 \omega_\alpha}{I} A_2^*(K_\alpha), A_3 = \frac{\rho B^4 \omega_\alpha^2}{I} A_3^*(K_\alpha), A_4 = \frac{\rho B^3 \omega_h^2}{I} A_4^*(K_h) \end{aligned} \quad (4)$$

Then we have:

$$\ddot{h}(t) + 2\xi_h \omega_h \dot{h}(t) + \omega_h^2 h(t) = H_1 \dot{h}(t) + H_2 \dot{\alpha}(t) + H_3 \alpha(t) + H_4 h(t) + \frac{1}{m} L_b(t) \quad (5a)$$

$$\ddot{\alpha}(t) + 2\xi_\alpha \omega_\alpha \dot{\alpha}(t) + \omega_\alpha^2 \alpha(t) = A_1 \dot{h}(t) + A_2 \dot{\alpha}(t) + A_3 \alpha(t) + A_4 h(t) + \frac{1}{I} M_b(t) \quad (5b)$$

Denote the buffeting displacement response as $\mathbf{x}(t) = [h(t), \alpha(t)]^T$ and the modified buffeting forces as $\mathbf{f}(t) = [\frac{1}{m} L_b(t), \frac{1}{I} M_b(t)]^T$, then Eq. (5) becomes:

$$\mathbf{M} = \begin{bmatrix} 1 & 0 \\ 0 & 1 \end{bmatrix}, \mathbf{C} = \begin{bmatrix} 2\xi_h \omega_h - H_1 & -H_2 \\ -A_1 & 2\xi_\alpha \omega_\alpha - A_2 \end{bmatrix}, \mathbf{K} = \begin{bmatrix} \omega_h^2 - H_4 & -H_3 \\ -A_4 & \omega_\alpha^2 - A_3 \end{bmatrix} \quad (6)$$

Considering that the fluctuations of wind speed $u(t)$ and $w(t)$ in Eq. (3) are random functions of time [19], Eq. (6) means that the bridge sectional model is a time-invariant linear system if the mean wind speed U is given. The frequency response function of the bridge sectional model is:

$$\mathbf{H}(\omega) = (\mathbf{K} - \omega^2 \mathbf{M} + i\omega \mathbf{C})^{-1} \quad (7)$$

where \mathbf{K} , \mathbf{M} , and \mathbf{C} are coupled stiffness matrix, mass matrix, and coupled damping matrix in Eq. (6), respectively; i is the imaginary unit; $\mathbf{H}(\omega)$ is the frequency response function at the specific circular frequency ω .

The PSD matrix of buffeting displacement response \mathbf{x} is:

$$\mathbf{S}_x(\omega) = \mathbf{H}(\omega) \mathbf{S}_f(\omega) \mathbf{H}^*(\omega) = \mathbf{H}(\omega) \begin{bmatrix} S_L(\omega) & 0 \\ 0 & S_M(\omega) \end{bmatrix} \mathbf{H}^*(\omega) \quad (8)$$

where $(\cdot)^*$ means the conjugate transpose of (\cdot) ; $\mathbf{S}_f(\omega) = \text{diag}[S_L(\omega), S_M(\omega)]$ means the PSD matrix of the modified buffeting lift force ($\frac{1}{m} L_b$) and modified moment force ($\frac{1}{I} M_b$) at circular frequency ω , respectively. Theoretically, $S_L(\omega)$ and $S_M(\omega)$ are not constant in the entire frequency band [51]. Also, the cross-spectrum of buffeting lift force and buffeting moment force is complicated [51], which is not considered in this study. This study finds that within a narrow frequency band $\mathcal{K} = \{k_1 \Delta\omega, (k_1 + 1) \Delta\omega, \dots, k_2 \Delta\omega\}$ ($0 < k_1 < k_2$) around the bridge sectional model's resonant circular frequency (i.e., ω_h and ω_α), the cross-spectrum of buffeting lift and moment forces can be neglected and $\mathbf{S}_f(\mathcal{K})$ can be considered as a constant matrix, which will not significantly influence the identification accuracy (as examined in Section 3). Similar solutions can also be found in Wu et al. [23]. Constant matrix $\mathbf{S}_f(\mathcal{K})$ can simplify the modeling procedure.

Then we can utilize $\mathbf{S}_x(\omega)$ to infer the FDs in the frequency domain. Denote all that we need to identify as the parameter vector θ :

$$\theta = [A_1^*, \dots, A_4^*, H_1^*, \dots, H_4^*, S_{L,1}, S_{M,1}, \dots, S_{L,d}, S_{M,d}]^T \quad (9)$$

where $d = 2$ in this study because the bridge sectional model is simplified as 2-DOF in Fig. 1 (d will be equal to 3 if the bridge sectional model is simplified as 3-DOF, i.e., when there are 18 FDs [52]).

Different from [30,53], the measurement noise is not considered here because we find that the contribution from measurement noise to the measured response PSDs in the wind tunnel is negligible. It can be proved by Figs. 16 and 22, where the reconstructed PSDs are consistent with the measured response PSDs even though the measurement noise is not considered. Neglecting the measurement noise in this study will not influence the identifying accuracy of FDs. On the other hand, the number of parameters to be inferred can also be reduced by neglecting the measurement noise, which increases the computational efficiency.

2.2. Spectral density estimator and complex Wishart distribution

Consider the stochastic vector process $\mathbf{x}(t) = [x_1(t), x_2(t), \dots, x_d(t)]^T$ and a finite number of discrete data $\mathbf{X}_N = \{\mathbf{x}(m), m = 0, 1, \dots, N-1\}$, where $d = 2$ in this study due to the 2-DOF bridge sectional model. Based on \mathbf{X}_N , the following discrete estimator of the spectral density matrix of the stochastic process $\mathbf{x}(t)$ is introduced [54]:

$$\mathbf{S}_{x,N}(\omega_k) = \mathcal{X}_N(\omega_k) \mathcal{X}_N^*(\omega_k) \quad (10)$$

where $\mathcal{X}_N(\omega_k)$ denotes the (scaled) Fourier Transform of the vector process \mathbf{x} at circular frequency ω_k , as follows:

$$\mathcal{X}_N(\omega_k) = \sqrt{\frac{\Delta t}{2\pi N}} \sum_{m=0}^{N-1} \mathbf{x}(m) \exp^{-i\omega_k m \Delta t} \quad (11)$$

where $\omega_k = k\Delta\omega$, $k = 0, 1, \dots, N_1 - 1$ with $N_1 = \text{INT}(\frac{N+1}{2})$ (denotes the ordinate at the Nyquist frequency), $\Delta\omega = \frac{2\pi}{T}$, and $T = N\Delta t$.

It is shown that the complex vector $\mathcal{X}_N(\omega_k)$ has a complex multivariate Gaussian distribution with zero mean as $N \rightarrow \infty$ [54,55]. Assume now that there is a set of M independent and identically distributed time histories whose realizations correspond to sampling data from the same process $\mathbf{x}(t)$ without overlapping. As $N \rightarrow \infty$, the corresponding frequency-domain stochastic processes $\mathcal{X}_N^{(m)}(\omega_k)$, $m = 1, 2, \dots, M$, are independent and follow an identical complex d -variate Gaussian distribution with zero mean [55]. Then, as $N \rightarrow \infty$ and if $M \geq d$, denote the average spectral density estimator as:

$$\mathbf{S}_N^M(\omega_k) = \frac{1}{M} \sum_{m=1}^M \mathbf{S}_N^{(m)}(\omega_k) \quad (12)$$

where $\mathbf{S}_N^M(\omega_k)$ follows a central complex Wishart distribution [43] of dimension d with M sets and the mean value $\mathbb{E}[\mathbf{S}_N^M(\omega_k)|\theta] = \mathbb{E}[\mathbf{S}_N(\omega_k)|\theta]$ [56]:

$$p[\mathbf{S}_N^M(\omega_k)|\theta] = \frac{\pi^{-d(d-1)/2} M^{M-d+d^2} |\mathbf{S}_N^M(\omega_k)|^{M-d}}{\left[\prod_{p=1}^d (M-p)! \right] \mathbb{E}[\mathbf{S}_N(\omega_k)|\theta]^M} \times \exp\left(-M \cdot \text{tr}\left\{\mathbb{E}[\mathbf{S}_N(\omega_k)|\theta]^{-1} \mathbf{S}_N^M(\omega_k)\right\}\right) \quad (13)$$

where the matrix $\mathbb{E}[\mathbf{S}_N(\omega_k)|\theta]$ is the theoretical matrix obtained by Eq. (8) given the parameter vector θ ; the matrix $\mathbf{S}_N^M(\omega_k)$ is obtained by Eq. (12), which is the measured PSD matrix by the wind tunnel test; $|\cdot|$ means the determinant of a matrix; $\text{tr}(\cdot)$ means the trace of a matrix; $p(\cdot)$ means the PDF. Actually, Eq. (13) links the theoretical PSD matrix $\mathbb{E}[\mathbf{S}_N(\omega_k)|\theta]$ with the measured PSD matrix $\mathbf{S}_N^M(\omega_k)$.

Furthermore, it has been investigated [53] that if $N \rightarrow \infty$, the matrices $\mathbf{S}_N^M(\omega_k)$ and $\mathbf{S}_N^M(\omega_l)$ are independently Wishart distributed for $k \neq l$, that is:

$$p[\mathbf{S}_N^M(\omega_k), \mathbf{S}_N^M(\omega_l)] = p[\mathbf{S}_N^M(\omega_k)] \cdot p[\mathbf{S}_N^M(\omega_l)] \quad (14)$$

Consider two frequency index sets $\mathcal{K}^{(1)} = \{k_1\Delta\omega, (k_1+1)\Delta\omega, \dots, k_2\Delta\omega\}$ ($k_1 < k_2$) (around ω_h) and $\mathcal{K}^{(2)} = \{k_3\Delta\omega, (k_3+1)\Delta\omega, \dots, k_4\Delta\omega\}$ ($k_2 \leq k_3 < k_4$) (around ω_a), then we can form the spectral set $\mathbf{S}_N^{M,\mathcal{K}^{(1)},\mathcal{K}^{(2)}} = [\mathbf{S}_N^M(k), k \in \{\mathcal{K}^{(1)}, \mathcal{K}^{(2)}\}]^T$. According to Eq. (14), we have:

$$p(\mathbf{S}_N^{M,\mathcal{K}^{(1)},\mathcal{K}^{(2)}}|\theta) = \prod_{k \in \mathcal{K}^{(1)}} p[\mathbf{S}_N^M(k)|\theta] \cdot \prod_{k \in \mathcal{K}^{(2)}} p[\mathbf{S}_N^M(k)|\theta] \quad (15)$$

where $p(\mathbf{S}_N^{M,\mathcal{K}^{(1)},\mathcal{K}^{(2)}}|\theta)$ is the likelihood function.

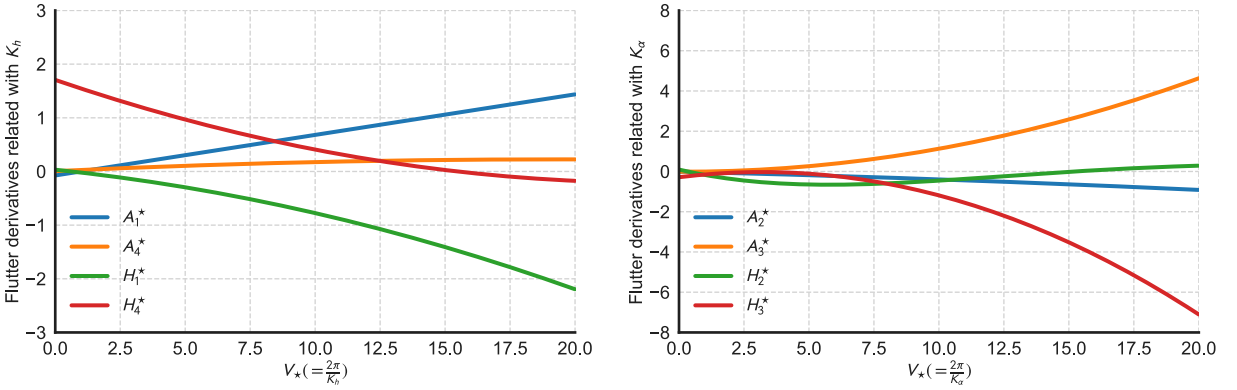


Fig. 2. Predefined flutter derivatives in the numerical simulations.

2.3. Posterior distributions of flutter derivatives

The parameter vector θ is actually a random vector during the process of inference, which is denoted as a random vector Θ with known prior distribution $p(\theta)$ ($\Theta \sim p(\theta)$) in this paper. Combining the prior $p(\theta)$ and the likelihood function $p(\mathbf{S}_N^{M, \mathcal{K}^{(1)}, \mathcal{K}^{(2)}} | \theta)$ in Eq. (15), under the context of Bayes' theorem [48], the posterior distribution of Θ is established:

$$p(\theta | \mathbf{S}_N^{M, \mathcal{K}^{(1)}, \mathcal{K}^{(2)}}) = \kappa p(\theta) \prod_{k \in \mathcal{K}^{(1)}} p[\mathbf{S}_N^M(k) | \theta] \cdot \prod_{k \in \mathcal{K}^{(2)}} p[\mathbf{S}_N^M(k) | \theta] \quad (16)$$

where κ is a normalizing constant [42]; $p(\theta | \mathbf{S}_N^{M, \mathcal{K}^{(1)}, \mathcal{K}^{(2)}})$ is the posterior distribution.

By Eq. (16), the most probable value (MPV) $\hat{\theta}$ is:

$$\hat{\theta} = \operatorname{argmax}_{\theta} [p(\theta | \mathbf{S}_N^{M, \mathcal{K}^{(1)}, \mathcal{K}^{(2)}})] \quad (17)$$

For individual component θ_i ($i = 1, 2, \dots, 12$), its marginal PDF can be calculated by integrating over the other components:

$$p(\theta_i | \mathbf{S}_N^{M, \mathcal{K}^{(1)}, \mathcal{K}^{(2)}}) = \int_{\Omega_{\Theta_{\sim i}}} p(\theta | \mathbf{S}_N^{M, \mathcal{K}^{(1)}, \mathcal{K}^{(2)}}) d\theta_{\sim i} \quad (18)$$

where $\theta_{\sim i}$ means the parameter vector θ excluding the i th parameter θ_i .

Practically [26,42], maximizing $p(\theta | \mathbf{S}_N^{M, \mathcal{K}^{(1)}, \mathcal{K}^{(2)}})$ is equivalent to minimizing the negative log-likelihood function $L(\theta)$ of Eq. (16). $L(\theta)$ is:

$$\begin{aligned} L(\theta) &= -\ln p(\theta | \mathbf{S}_N^{M, \mathcal{K}^{(1)}, \mathcal{K}^{(2)}}) = -\ln \left\{ \kappa p(\theta) \prod_{k \in \mathcal{K}^{(1)}} p[\mathbf{S}_N^M(k) | \theta] \cdot \prod_{k \in \mathcal{K}^{(2)}} p[\mathbf{S}_N^M(k) | \theta] \right\} \\ &\propto M \left\{ \sum_{k=k_1}^{k_2} \ln \left| \mathbb{E} [\mathbf{S}_N(k \Delta \omega) | \theta] \right| + \sum_{k=k_1}^{k_2} \operatorname{tr} \left[\mathbb{E} [\mathbf{S}_N(k \Delta \omega) | \theta]^{-1} \mathbf{S}_N^M(k \Delta \omega) \right] \right. \\ &\quad \left. + \sum_{k=k_3}^{k_4} \ln \left| \mathbb{E} [\mathbf{S}_N(k \Delta \omega) | \theta] \right| + \sum_{k=k_3}^{k_4} \operatorname{tr} \left[\mathbb{E} [\mathbf{S}_N(k \Delta \omega) | \theta]^{-1} \mathbf{S}_N^M(k \Delta \omega) \right] \right\} - \ln p(\theta) \end{aligned} \quad (19)$$

Equivalently, the MPV $\hat{\theta}$ is:

$$\hat{\theta} = \operatorname{argmax}_{\theta} [p(\theta | \mathbf{S}_N^{M, \mathcal{K}^{(1)}, \mathcal{K}^{(2)}})] = \operatorname{argmin}_{\theta} [L(\theta)] \quad (20)$$

To validate the identified FDs, we can reconstruct the PSDs of buffeting displacement responses with MPV $\hat{\theta}$ and examine the consistency between the reconstructed PSDs and the measured PSDs. We propose a nondimensional indicator λ to examine the consistency [57], as shown in Eq. (21). The closer λ is to 1, the more accurate is the MPV $\hat{\theta}$. By numerical verification, we find that $\lambda > 0.8$ can usually guarantee the identified accuracy.

$$\lambda = \frac{(n \sum_k \{ \mathbb{E} [\mathbf{S}_N(k) | \hat{\theta}] \mathbf{S}_N^M(k) \} - \sum_k \mathbb{E} [\mathbf{S}_N(k) | \hat{\theta}] \cdot \sum_k \mathbf{S}_N^M(k))^2}{\left(n \sum_k (\mathbb{E} [\mathbf{S}_N(k) | \hat{\theta}])^2 - (\sum_k \mathbb{E} [\mathbf{S}_N(k) | \hat{\theta}])^2 \right) \left(n \sum_k (\mathbf{S}_N^M(k))^2 - (\sum_k \mathbf{S}_N^M(k))^2 \right)} \quad (21)$$

where $k \in \{\mathcal{K}^{(1)}, \mathcal{K}^{(2)}\}$; n is the number of elements in $\{\mathcal{K}^{(1)}, \mathcal{K}^{(2)}\}$; $\mathbb{E} [\mathbf{S}_N(k) | \hat{\theta}]$ is the reconstructed PSD with identified MPVs $\hat{\theta}$ at frequency k ; $\mathbf{S}_N^M(k)$ is the measured PSD at frequency k .

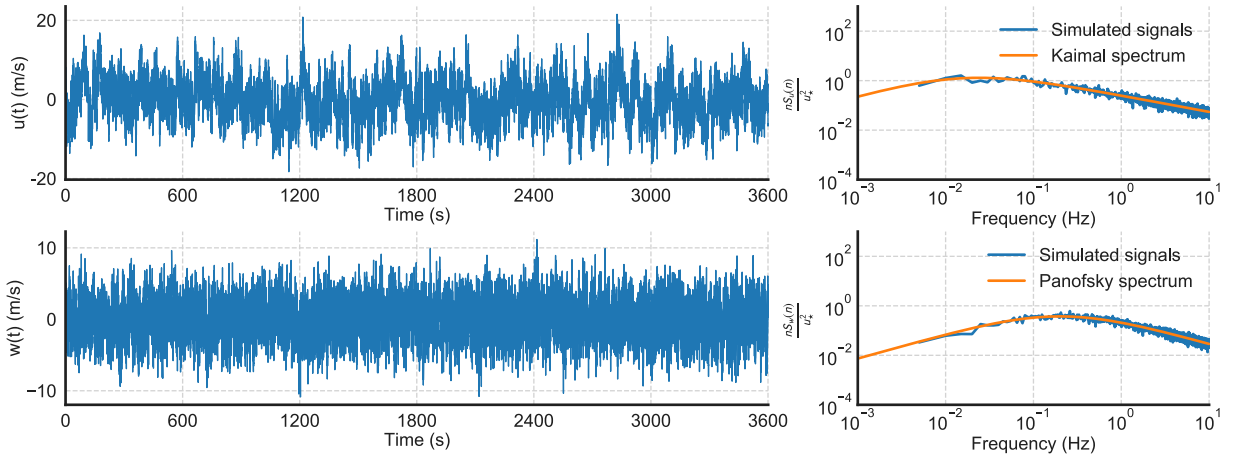


Fig. 3. Time histories of fluctuating wind speeds when $U(50) = 40$ m/s.

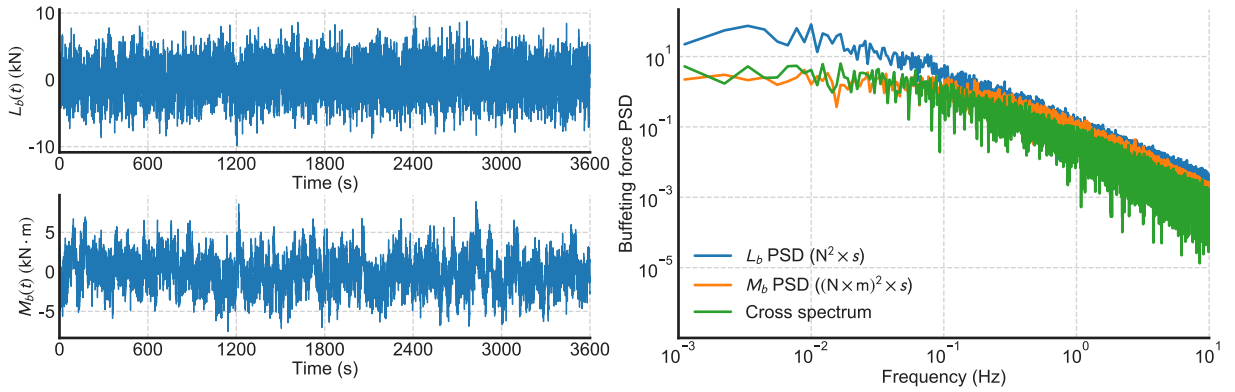


Fig. 4. Time histories of vertical buffeting force $L_b(t)$ and torsional buffeting force $M_b(t)$ when $U(50) = 40$ m/s.

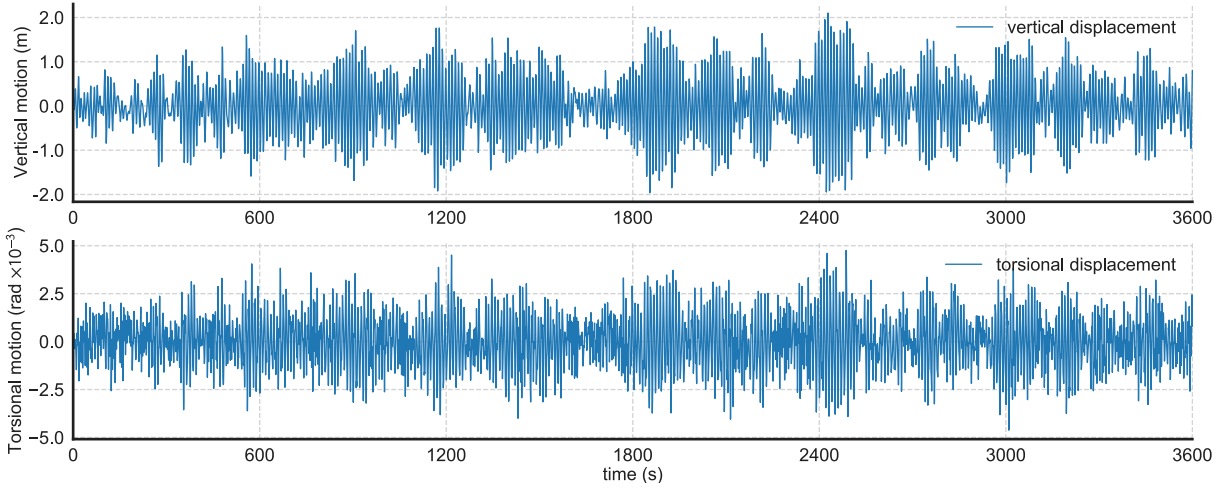


Fig. 5. Time histories of vertical buffeting displacement $h(t)$ and torsional buffeting displacement $\alpha(t)$ when $U(50) = 40$ m/s ($K_h = 0.5655$ and $K_\alpha = 1.4137$).

For a globally identifiable model updating problem, the MPV can be estimated by numerically maximizing the posterior PDF, which can be well approximated by a multi-variable Gaussian distribution [42]. However, the actual form of the posterior PDF

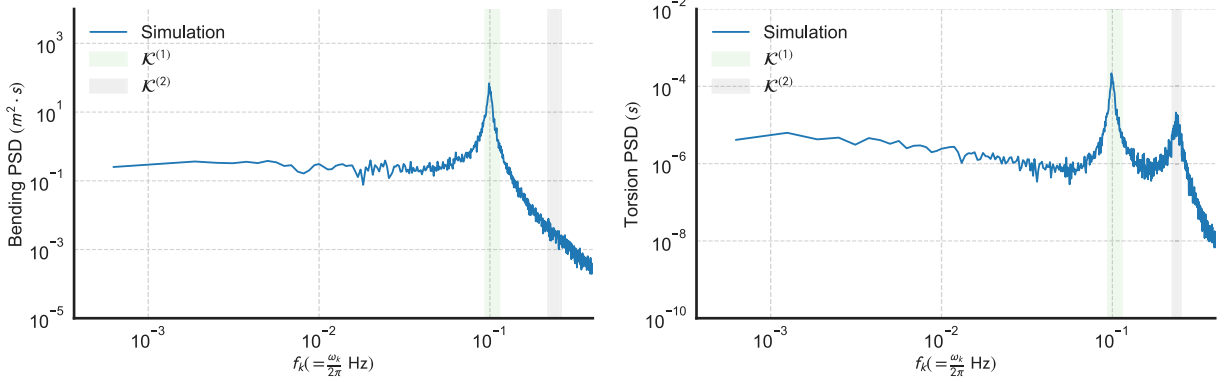


Fig. 6. Simulated PSDs of buffeting displacement responses when $U(50) = 40$ m/s ($K_h = 0.5655$ and $K_a = 1.4137$).

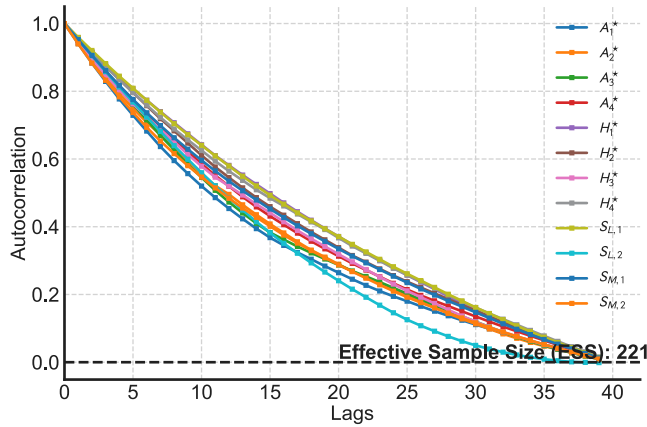


Fig. 7. MCMC autocorrelation (case of simulation).

$p(\theta | \mathbf{S}_N^{M, \mathcal{K}^{(1)}, \mathcal{K}^{(2)}})$ in this study is too complicated to be described as Gaussian distribution. One popular solution is based on Markov chain Monte Carlo (MCMC) sampling [58,59]. The basic idea of MCMC is to construct stationary chains of samples, and the posterior is the invariant distribution of the Markov chain if the transition probability $\pi(\theta^{(t+1)} | \theta^{(t)})$ fulfills the detailed balance condition

$$p(\theta^{(t)} | \mathbf{S}_N^{M, \mathcal{K}^{(1)}, \mathcal{K}^{(2)}}) \pi(\theta^{(t+1)} | \theta^{(t)}) = p(\theta^{(t+1)} | \mathbf{S}_N^{M, \mathcal{K}^{(1)}, \mathcal{K}^{(2)}}) \pi(\theta^{(t)} | \theta^{(t+1)}) \quad (22)$$

In this study, AIES-based algorithm [49] is adopted to better accommodate the potential strong correlation among the parameters within the posterior distribution. The affine invariance property is achieved by generating proposals according to stretch move [49]. This refers to proposing a new candidate by

$$\theta_i^{(*)} = \theta_i^{(t)} + Z (\theta_j^{(t)} - \theta_i^{(t)}), \text{ where } Z \sim p(z) = \begin{cases} \frac{1}{\sqrt{z}(2\sqrt{a} - \frac{2}{\sqrt{a}})} & \text{if } z \in [1/a, a] \\ 0 & \text{otherwise} \end{cases} \quad (23)$$

This requires sampling from the distribution $p(z)$ defined by the tuning parameter $a > 1$ (practically $a = 2$ [48,49]). The acceptance rate $\alpha(\theta_i^{(*)}, \theta_i^{(t)})$ is

$$\alpha(\theta_i^{(*)}, \theta_i^{(t)}) = \min \left\{ 1, z^{n-1} \frac{p(\theta_i^{(*)} | \mathbf{S}_N^{M, \mathcal{K}^{(1)}, \mathcal{K}^{(2)}})}{p(\theta_i^{(t)} | \mathbf{S}_N^{M, \mathcal{K}^{(1)}, \mathcal{K}^{(2)}})} \right\} \quad (24)$$

where n is the dimension of the parameter space.

The convergence criteria for the posterior distributions of all model parameters are measured by autocorrelation, and MCMC will converge if the autocorrelation of each parameter gradually approaches zero during sampling [60]. By MCMC, the posterior distribution $p(\theta | \mathbf{S}_N^{M, \mathcal{K}^{(1)}, \mathcal{K}^{(2)}})$ can be evaluated efficiently.

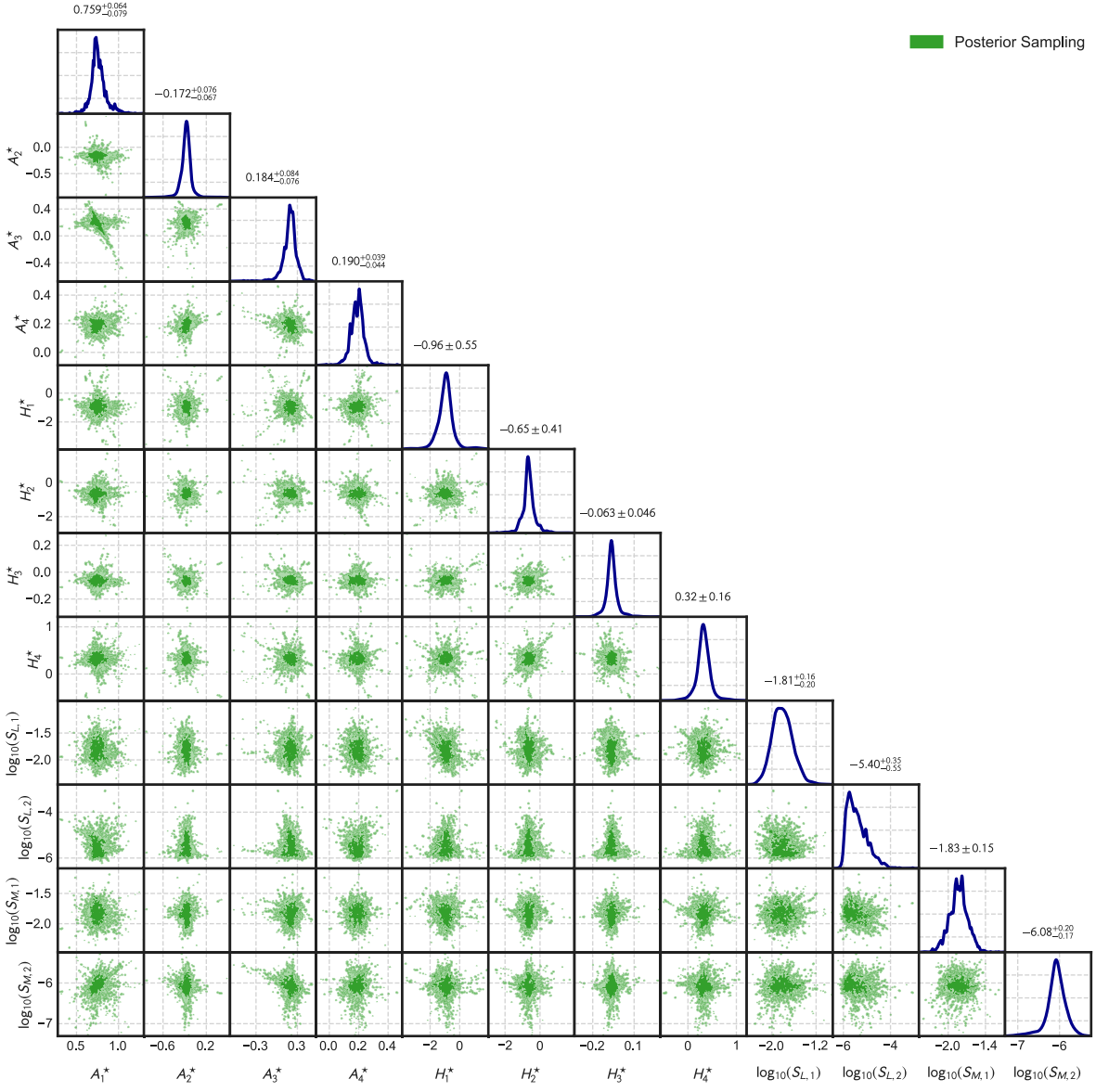


Fig. 8. Posterior distributions of FDs and buffeting force PSDs when $U(50) = 40$ m/s ($K_h = 0.5655$ and $K_a = 1.4137$).

3. Numerical simulations

To verify the feasibility of the Bayesian spectral density approach [42], numerical simulations are carried out in this section.

3.1. Predefined modal properties and FDs

The vertical and torsional frequencies are set as $f_h = 0.1$ Hz and $f_a = 0.25$ Hz, respectively. Both damping ratios are set as 0.005. The bridge deck is 36 m. The mass per unit length is 27935 kg/m. The mass moment of inertia per unit length is 2595580 kg \times m²/m. The air density is 1.225 kg/m³. The predefined FDs are shown in Fig. 2, where V_* means the reduced velocity, K_h and K_a are the reduced frequencies as described in Section 2.1.

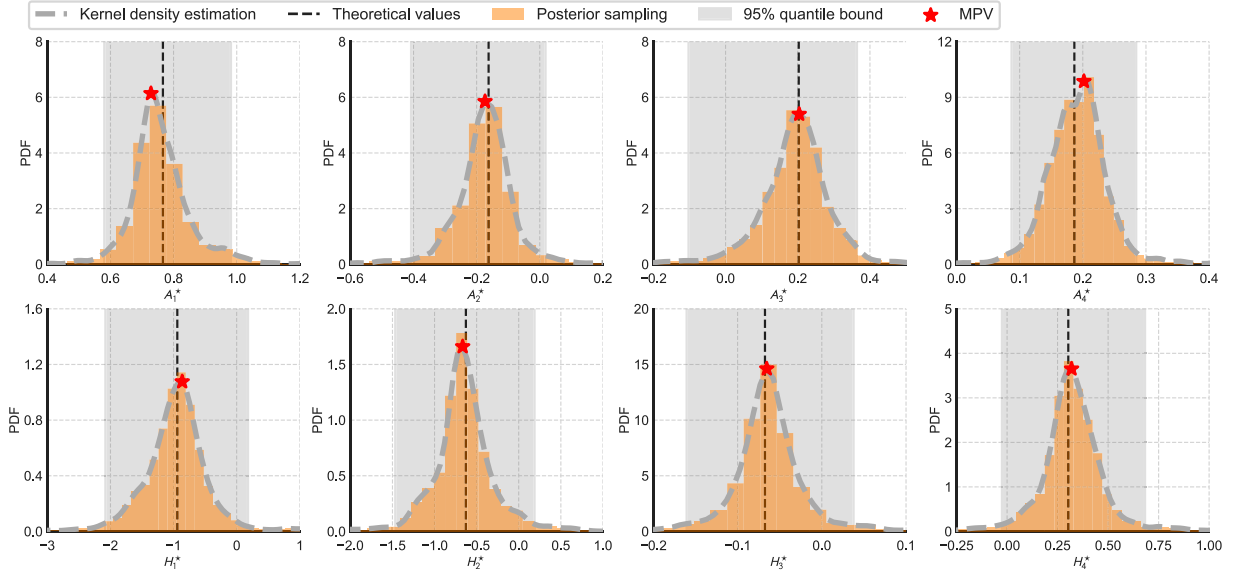


Fig. 9. Posterior marginal distributions of FDs when $U(50) = 40$ m/s ($K_h = 0.5655$ and $K_a = 1.4137$).

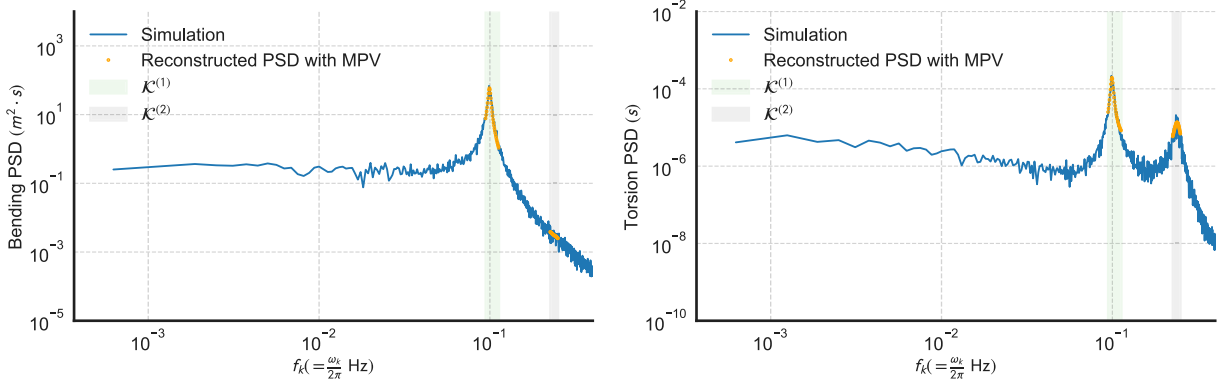


Fig. 10. Comparison between the reconstructed PSDs (with identified MPVs of A_i^* , H_i^* , $i = 1, 2, 3, 4$, and $S_{L,1}$, $S_{L,2}$, $S_{M,1}$, $S_{M,2}$) and the theoretical PSDs when $U(50) = 40$ m/s ($K_h = 0.5655$ and $K_a = 1.4137$) with the indicator $\lambda = 0.9421$.

3.2. Buffeting displacement response

In order to illustrate if the simplification in Eq. (8) (i.e., neglecting the cross spectrum of buffeting forces along two directions) is reasonable, in this subsection, we employ Kaimal spectrum [61] (Eq. (25a)) in u direction and Panofsky spectrum [62] (Eq. (25b)) in w direction to generate time histories of fluctuating wind speed based on the method proposed by Shinozuka and Jan [63], and then generate time histories of two buffeting forces (have a correlation) by Eq. (3).

$$\frac{nS_u(n)}{u_*^2} = \frac{200f}{(1+50f)^{5/3}} \quad (25a)$$

$$\frac{nS_w(n)}{u_*^2} = \frac{6f}{(1+4f)^2} \quad (25b)$$

$$f = \frac{nZ}{U(Z)} \quad (25c)$$

$$u_* = \frac{KU(Z)}{\ln \frac{Z}{Z_0}} \quad (25d)$$

where n is the frequency of wind speed, unit of which is Hz; $S_u(n)$ and $S_w(n)$ are PSDs of fluctuating wind speeds along u and w directions, respectively; K is a nondimensional constant (assumed as 0.4 here); z_0 is the height of ground roughness (assumed as

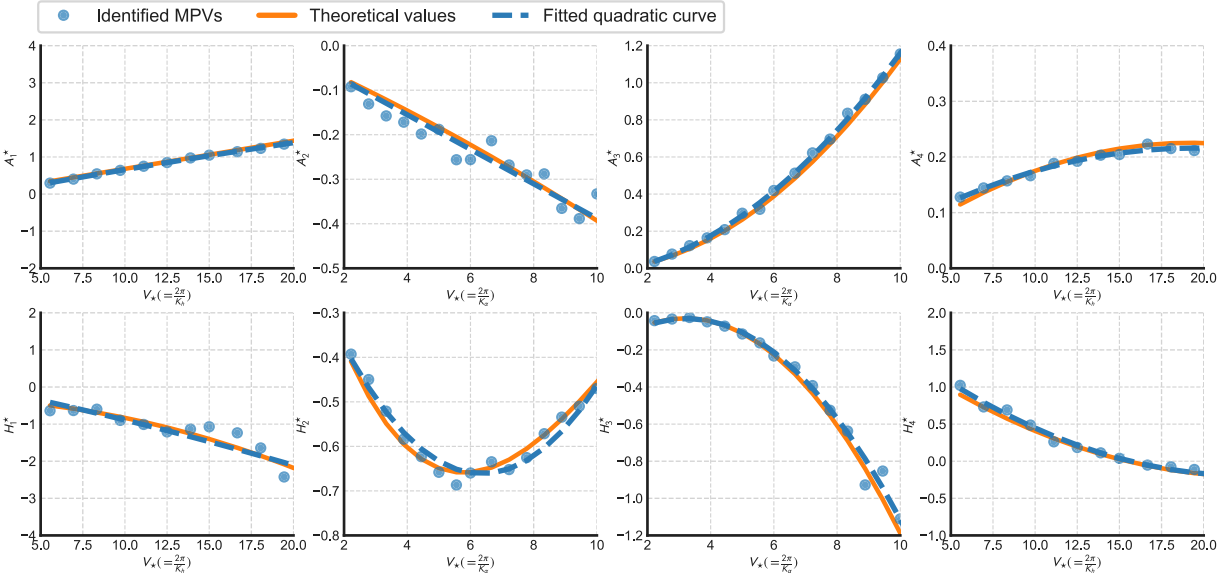


Fig. 11. MPVs and corresponding uncertainty of identified FDs at various reduced velocities.

0.03 m here); Z is the height of the bridge deck (assumed as 50 m here); $U(Z)$ is the mean wind speed at the height of Z ; u_* is the airflow frictional velocity.

Take $U(50) = 40$ m/s for example. The simulated time histories of fluctuating wind speeds are shown in Fig. 3, where the simulated Kaimal spectrum and Panofsky spectrum can also be found.

The buffeting forces $L_b(t)$ and $M_b(t)$ in Eq. (3) can then be generated, as shown in Fig. 4. The auto-spectral densities of $L_b(t)$ and $M_b(t)$ and the amplitude of their cross-spectral density are also shown in Fig. 4.

The response time series are generated by “lsim” function with MATLAB, where the sampling interval is 0.02 s (i.e., $f_s = 50$ Hz). Fig. 5 shows an example of vertical and torsional displacements when the mean wind speed $U(50) = 40$ m/s (i.e., $K_h = 0.5655$ and $K_a = 1.4137$).

As shown in Fig. 6, the selected frequency set $\mathcal{K}^{(1)}$ is 0.08Hz~0.12Hz, $\mathcal{K}^{(2)}$ is 0.22 Hz~0.26 Hz. In Fig. 6, the blue continuous line is plotted by the simulated signals with Eq. (12). The M in Eq. (12) is set as 10.

3.3. MCMC sampling

3.3.1. Prior distributions

The determination of the prior distributions is important for the calculation and convergence of posterior distributions [42]. For FDs A_i^* , H_i^* ($i = 1, 2, 3, 4$) and modified buffeting force PSDs $S_{L,1}$, $S_{L,2}$, $S_{M,1}$, $S_{M,2}$, the prior distributions are assumed to obey the uniform distribution (i.e., there are no prior information) independently.

Bayesian inference is utilized to quantify uncertainties, and AIES-based MCMC sampling is adopted to estimate the posterior PDF of the input parameters [49,64]. AIES-based MCMC sampling is set to run 100,000 samples, thinning by taking every 10th sample and a burn-in of 20% total samples is employed.

3.3.2. Convergence diagnostics

To diagnose convergence of Markov chain, Fig. 7 shows that the autocorrelations of the input parameters approach zero when lags = 38, which means that the Markov chains converge [60].

3.3.3. Posterior distributions

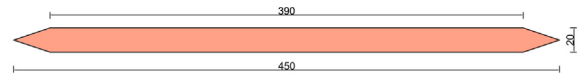
Fig. 8 illustrates the posterior distributions of Θ . The numerical simulation shows that FDs (A_i^* , H_i^* , $i = 1, 2, 3, 4$) are approximately mutually independent. Since this study focuses on FDs, the following content will not discuss the MPVs and corresponding uncertainty of buffeting force PSDs.

3.3.4. Marginal distributions of flutter derivatives and reconstruction of buffeting responses' PSDs

Fig. 9 shows the posterior marginal distributions and 95% quantile bounds, where the kernel density estimation (KDE) is adopted to get the MPVs (position with the largest probability) [65]. The MPVs are consistent with the theoretical values generally for each input parameter, where the small deviations that exist in A_1^* and A_4^* may be caused by aliasing and leakage of the simulated signals [26,42].



(a) Thin plate model with regularly-arranged grids



(b) Cross sectional shape of the thin plate model

Fig. 12. Case 1: the thin plate model.

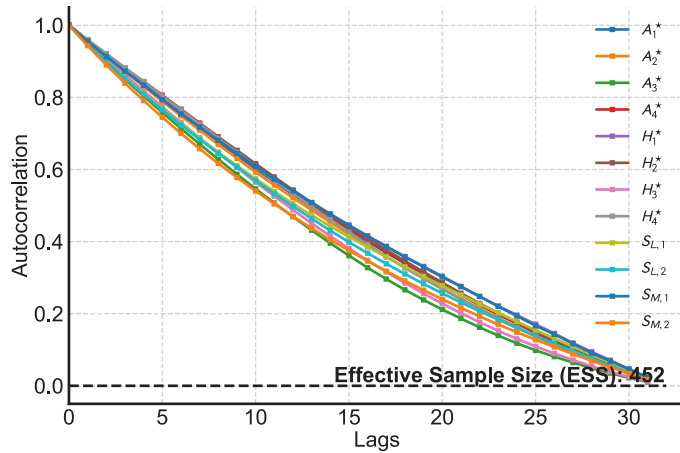


Fig. 13. Case 1: MCMC autocorrelation.

Fig. 10 shows the reconstruction of buffeting responses' PSDs with the identified MPVs of A_i^* , H_i^* ($i = 1, \dots, 4$), $S_{L,1}$, $S_{L,2}$, $S_{M,1}$ and $S_{M,2}$. It is clear that though some small deviation exists in Fig. 9, the reconstructed PSDs are still consistent with the theoretical ones, where the indicator $\lambda = 0.9421$.

3.4. Most probable values (MPVs) of FDs at various reduced velocities

Fig. 11 shows the comparison between identified FDs' MPVs and corresponding predefined theoretical values. The identified MPVs are consistent with the predefined theoretical values at various reduced velocities in general.

4. Wind tunnel tests

To evaluate the feasibility of Bayesian spectral density approach in extracting FDs of bridge sectional model in turbulent flow, the wind tunnel tests of a streamlined thin plate model and a center-slotted girder sectional model are carried out, respectively. The thin plate is employed because there are theoretical solutions, i.e., Theodorsen functions [66], of this shape. The center-slotted girder section is employed because this kind of cross sectional shape is widely utilized in current engineering practice for the construction of long-span bridges. The wind tunnel tests are carried out in TJ-1 wind tunnel at Tongji University in China. TJ-1 is an open straight-through-type boundary layer wind tunnel with a working section of 1.8 m(width)×1.8 m(height), and the wind speed can be continuously operated within the range of 0.5 ~ 25 m/s.

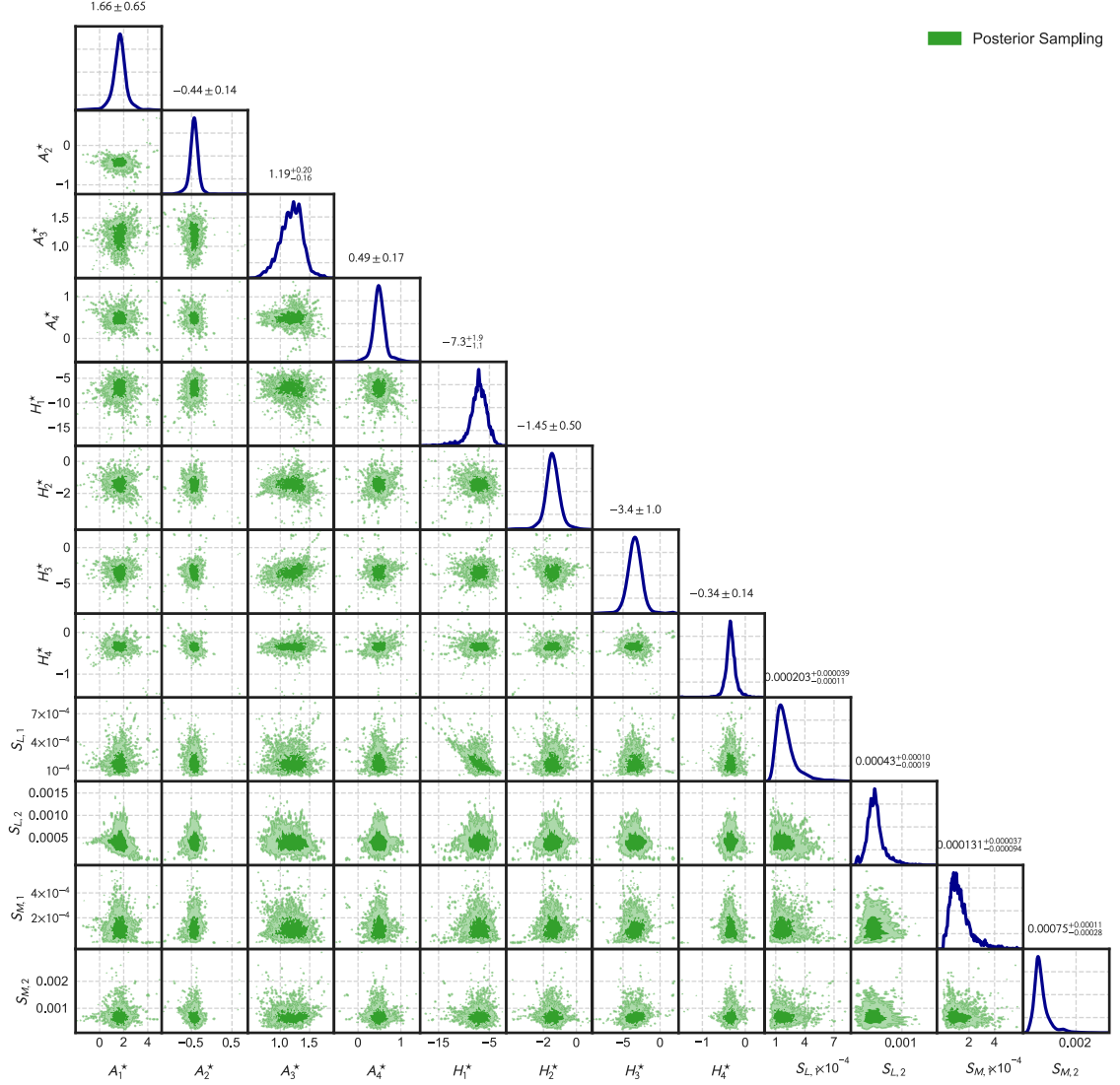


Fig. 14. Case 1: posterior distributions of flutter derivatives of the thin plate when $U = 8.6$ m/s ($K_h = 0.6247$, $K_a = 1.0028$).

4.1. Case 1: thin plate model

The FDs of a thin plate can be derived theoretically (i.e., Theodorsen function [66]). As a result, a thin plate model is tested to verify the Bayesian spectral density approach, where the Theodorsen results are given as follows [66]:

$$H_1^* = \frac{-\pi F(k)}{2k}, H_2^* = \frac{-\pi}{8k} \left[1 + F(k) + \frac{2G(k)}{k} \right], H_3^* = \frac{-\pi}{4k^2} \left[F(k) - \frac{k \cdot G(k)}{2} \right], H_4^* = \frac{\pi}{4} \left[1 + \frac{2G(k)}{k} \right] \quad (26a)$$

$$A_1^* = \frac{\pi F(k)}{8k}, A_2^* = \frac{-\pi}{32k} \left[1 - F(k) - \frac{2G(k)}{k} \right], A_3^* = \frac{\pi}{16k^2} \left[\frac{k^2}{8} + F(k) - \frac{k \cdot G(k)}{2} \right], A_4^* = \frac{-\pi G(k)}{8k} \quad (26b)$$

$$F(k) = 1 - \frac{0.165}{1 + \left(\frac{0.0455}{k} \right)^2} - \frac{0.335}{1 + \left(\frac{0.3}{k} \right)^2}, \quad G(k) = -\frac{\frac{0.165 \times 0.0455}{k}}{1 + \left(\frac{0.0455}{k} \right)^2} - \frac{\frac{0.335 \times 0.3}{k}}{1 + \left(\frac{0.3}{k} \right)^2} \quad (26c)$$

where $k = \frac{\omega_B}{2U} = \frac{K}{2}$, B is the width of the sectional model, K is the reduced frequency.

As shown in Fig. 12(a), the turbulent flow was generated by regularly-arranged grids, where the thin plate model was suspended by eight springs. The thin plate model is centrally-symmetric with 1.745 m in the longitudinal dimension. As shown in Fig. 12(b),

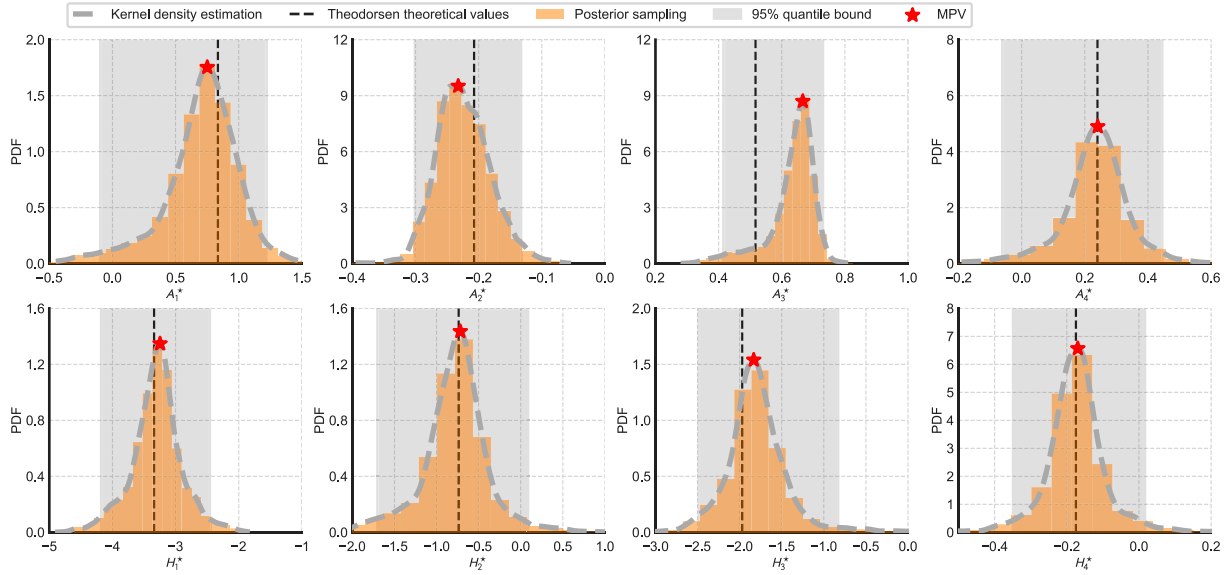


Fig. 15. Case 1: posterior marginal distributions of flutter derivatives of the thin plate when $U = 8.6$ m/s ($K_h = 0.6247$, $K_a = 1.0028$).

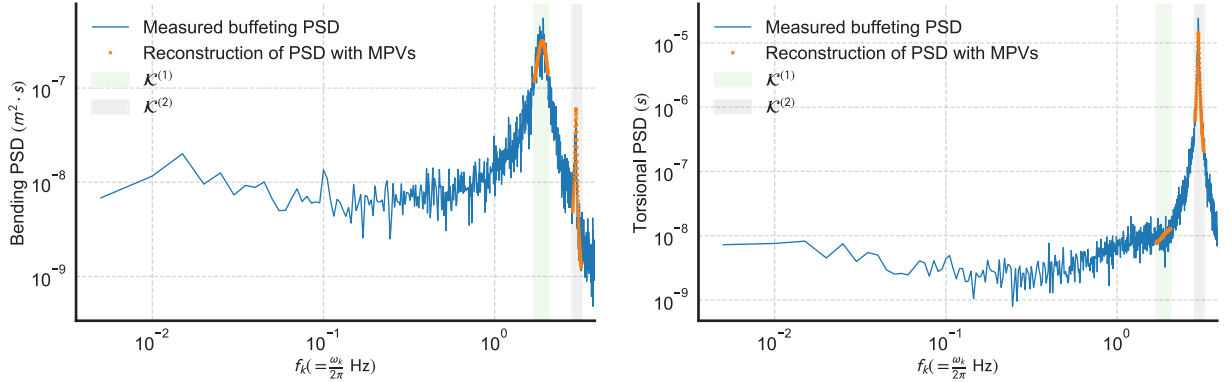


Fig. 16. Case 1: measured buffeting displacement PSDs and reconstruction of PSDs with identified MPVs of FDs and buffeting force PSDs when $U = 8.6$ m/s ($K_h = 0.6247$, $K_a = 1.0028$) with $\lambda = 0.9367$.

the size of the cross section is $450 \text{ mm} \times 20 \text{ mm}$ (length \times height). The mass is 6 kg/m ; the mass moment of inertia is $0.7 \text{ kg} \times \text{m}^2/\text{m}$; the vertical modal frequency is 1.9 Hz , the vertical damping ratio is 0.004 ; the torsional modal frequency is 3.05 Hz , the torsional damping ratio is 0.003 .

The detailed identification process has been discussed in Section 3. In this subsection, we take the condition of the mean wind speed $U = 8.6 \text{ m/s}$ for example to explain the identification process of the thin plate. The sampling rate is 1024 Hz . Conventionally with the previous least square method [13] in the free vibration test, the sampling duration is $10 \text{ s} \sim 20 \text{ s}$. When utilizing the buffeting response, the sampling duration is usually much longer (e.g., 14 min with stochastic subspace identification technology in [19]). In order to obtain reliable and stable measured PSDs, the sampling duration in the case of thin plate model is 2000 s , M in Eq. (13) is 8.

Fig. 13 shows that the Markov chain has converged since the autocorrelation of each parameter in θ approaches zero when lags = 31.

As shown in Fig. 14, for the thin plate, the FDs are approximately independent with each other in a single test. It should be stressed again that the variances shown in each posterior FD sampling, namely identification uncertainty here, are different from the experimental uncertainties examined in [24,67]. The variances of each FD in this study actually stand for the posterior marginal distributions, which heavily depends on the prior information [42] and the condition of the measured signals [26]. We can also obtain the experimental uncertainties through the proposed Bayesian spectral density approach by statistical analysis of the FDs' MPVs in many tests with the same preset experimental conditions. Furthermore, the correlation of each FD in this study is also different from that of experimental uncertainties due to the same reason.

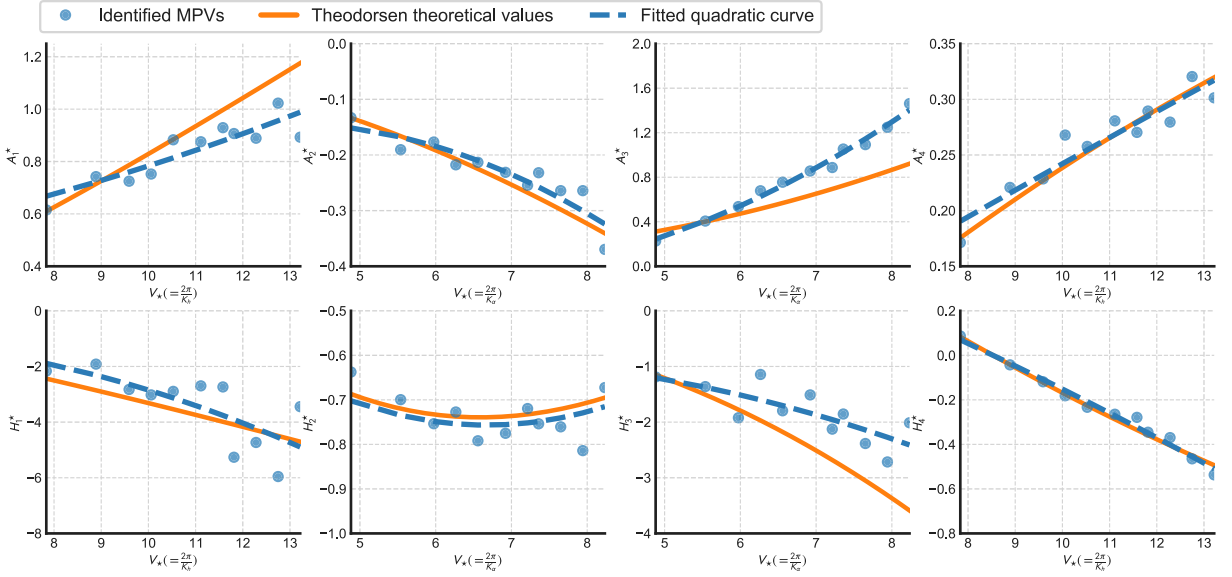
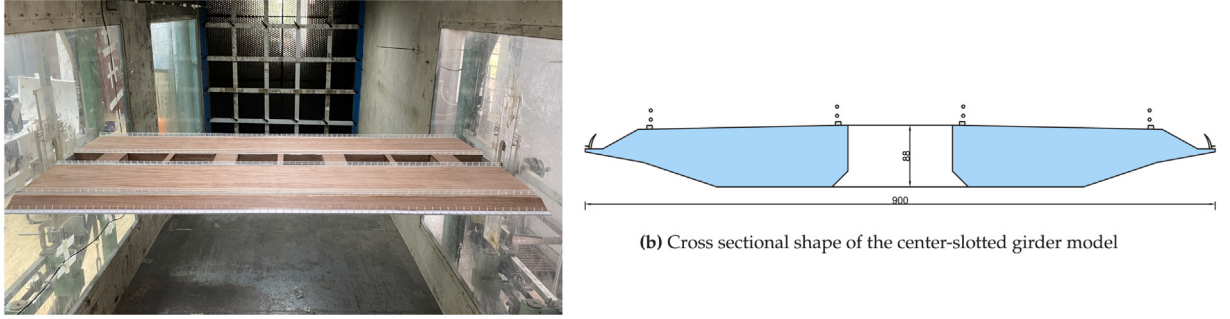


Fig. 17. Case 1: identified MPVs and corresponding uncertainty of flutter derivatives of the thin plate at various reduced velocities.



(a) Center-slotted girder model with regularly-arranged grids

Fig. 18. Case 2: the center-slotted girder model.

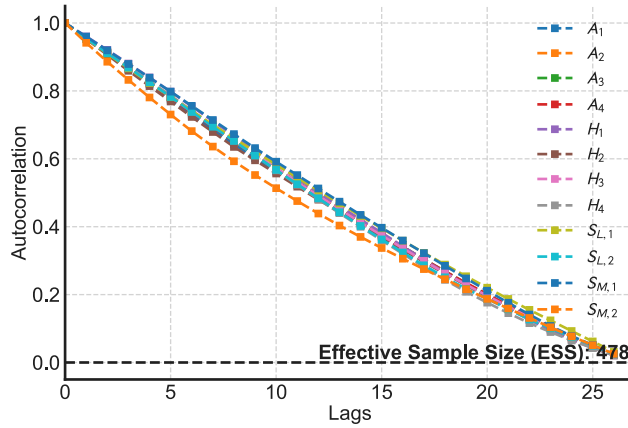


Fig. 19. Case 2: MCMC autocorrelation.

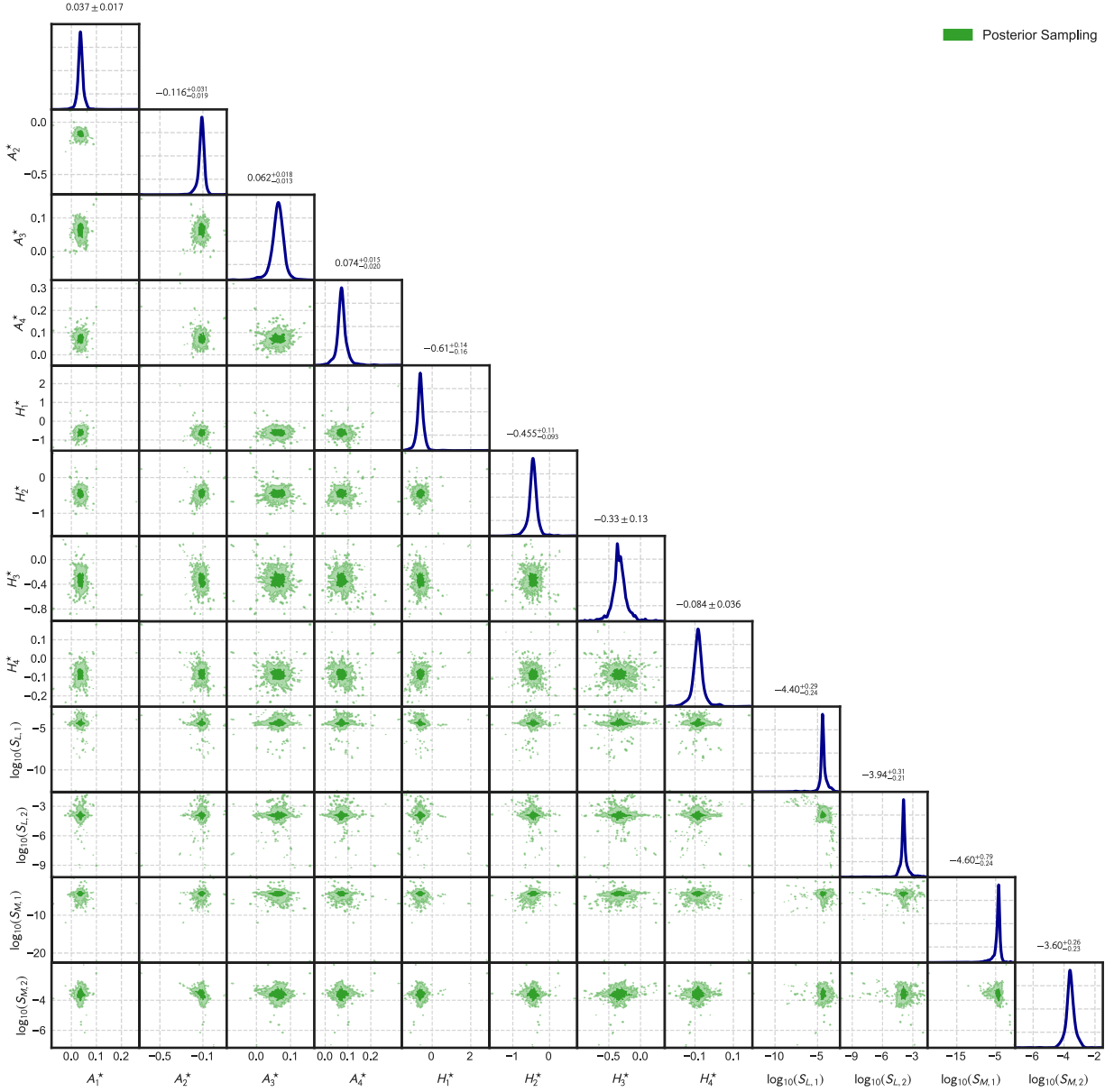


Fig. 20. Case 2: posterior distributions of flutter derivatives and buffeting force PSDs of the center-slotted girder model when $U = 7.25$ m/s ($K_h = 1.4547$, $K_a = 2.3399$).

Fig. 15 shows the posterior marginal distributions of each FD, where the 95% quantile bounds are also given. The dashed vertical line means the Theodorsen theoretical values, we can notice that the identified MPVs are generally consistent with the Theodorsen values. Some bias is observed in A_3^* , reason of which is perhaps that the thin plate is not the rigorous infinite thin plate so the “true” value is not strictly the Theodorsen solution. Similar bias can also be found in [18].

Fig. 16 shows the reconstructed buffeting displacement PSDs with identified MPVs of FDs and buffeting force PSDs. The reconstructed PSDs are consistent with the measured ones (with $\lambda = 0.9367$), which can also prove that the identified FDs are correct. Specially, for a general bridge cross section (i.e., there are no theoretical values of FDs for reference), one of the most efficient method to validate the identified MPVs is to reconstruct the buffeting displacement PSDs and compare those with the measured ones by using the indicator λ .

Fig. 17 shows the identified MPVs of FDs at various reduced velocities. The blue dashed line is the fitted quadratic curve with identified MPVs of FDs. Generally, the identified MPVs of FDs are consistent with the Theodorsen theoretical values. Again, identified A_3^* and H_3^* are relatively higher than the Theodorsen values since the thin plate model is not perfectly infinite. Similar bias can also be found when the FDs are extracted by stochastic subspace identification technology [18].

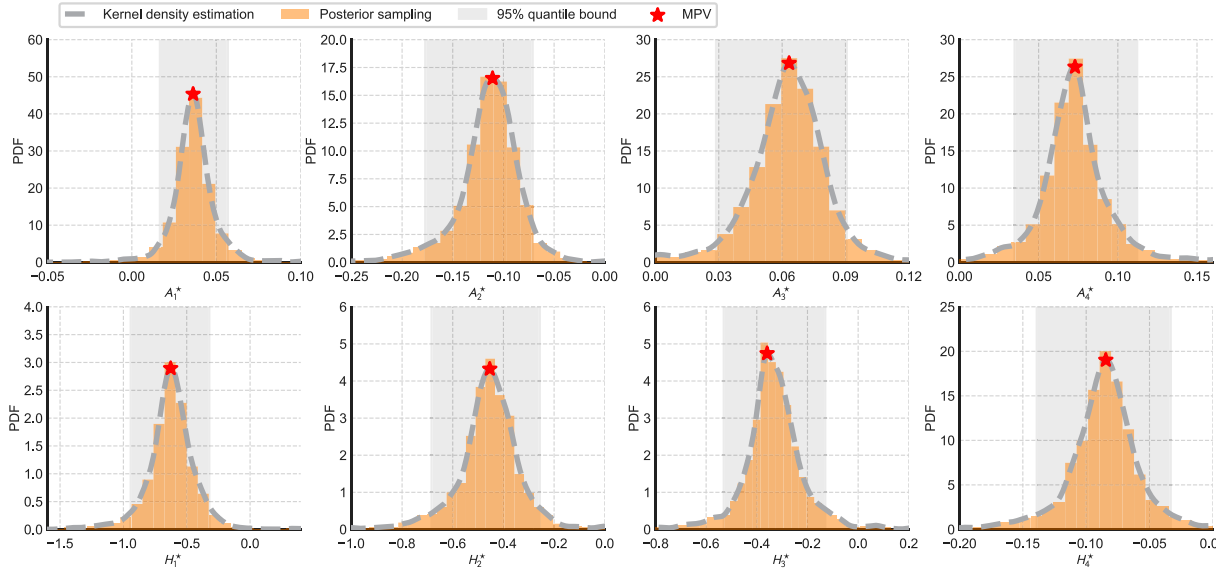


Fig. 21. Case 2: posterior marginal distribution of flutter derivatives of the center-slotted girder model when $U = 7.25$ m/s ($K_h = 1.4547$, $K_a = 2.3399$).

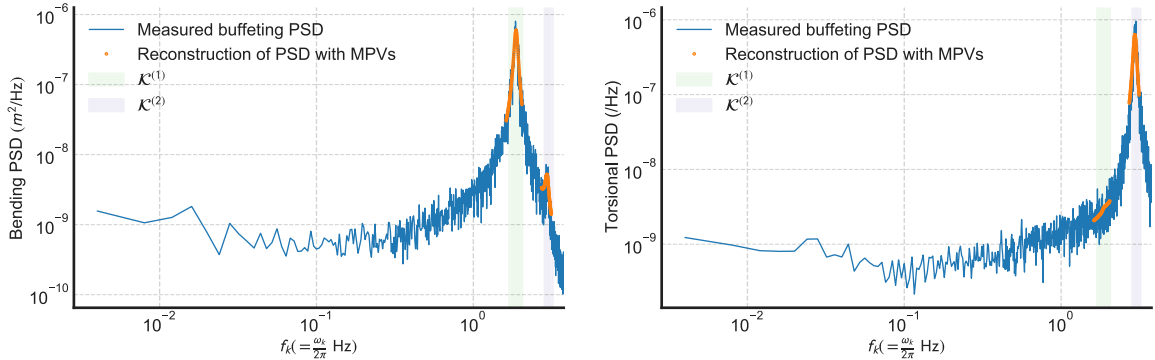


Fig. 22. Case 2: measured buffeting displacement PSDs and reconstruction of PSDs with identified MPVs of FDs and buffeting force PSDs when $U = 7.25$ m/s ($K_h = 1.4547$, $K_a = 2.3399$) with $\lambda = 0.9679$.

4.2. Case 2: sectional model of a center-slotted girder

In order to investigate the applicability of the proposed Bayesian spectral density approach towards the general bridge cross section, we choose the widely-utilized center-slotted girder. Fig. 18 shows the cross section of the center-slotted girder. It is 1.745 m in the longitudinal dimension. The size of the cross section is 900 mm × 88 mm (length×height). The mass is 11.7 kg/m; the mass moment of inertia is 1.7 kg × m²/m; the vertical modal frequency is 1.86 Hz, the vertical damping ratio is 0.002; the torsional modal frequency is 3.00 Hz, the torsional damping ratio is 0.0015. The sampling rate is 1024 Hz. The sampling duration in the case of center-slotted girder model is 2000 s, M in Eq. (13) is 8.

In the case of center-slotted girder model, take the mean wind speed $U = 7.25$ m/s for example. Fig. 19 shows that the autocorrelation approaches zero when lags = 27, which means the Markov chain converges.

Fig. 20 shows the posterior samplings, where the FDs are independent with each other in a single test.

Fig. 21 shows the posterior marginal distributions of FDs, where the 95% quantile bounds are also given.

Fig. 22 shows the measured buffeting displacement PSDs and the reconstructed PSDs with identified MPVs, where a good consistency is found with $\lambda = 0.9679$. In practice, comparison between the measured PSDs and the reconstructed PSDs is of vital importance for the identification process of a general bridge section, which is an efficient method to verify the identified results.

Fig. 23 shows the identified MPVs of FDs at various reduced velocities by the Bayesian spectral density approach in turbulent flow versus the least square method in uniform flow with free vibration data. The orange dashed lines are quadratic curves fitted by the identified MPVs at various reduced velocities of the Bayesian spectral density approach. Except A_1^* , the other FDs are consistent when identified by two different methods. The latent reasons for the deviation in A_1^* need to be investigated further in the future.

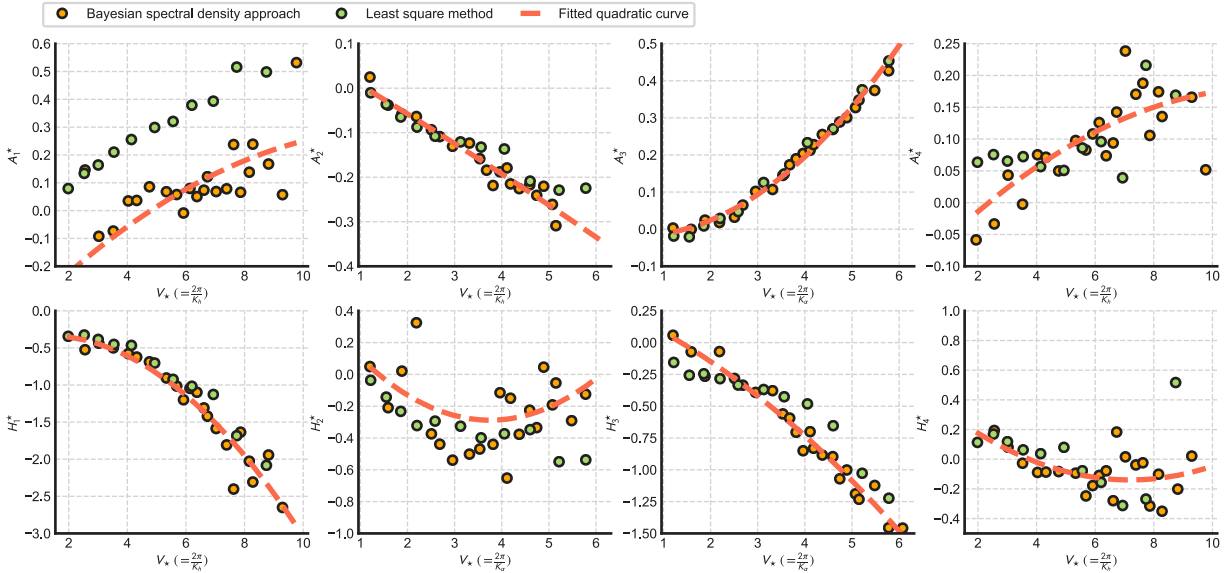


Fig. 23. Case 2: identified MPVs of flutter derivatives of the center-slotted girder model at various reduced velocities by Bayesian spectral density approach in turbulent flow versus least square method in uniform flow.

Anyway, the bias in A_1^* does not affect the reconstruction of buffeting displacement PSDs due to the consistency ($\lambda = 0.9679$) shown in Fig. 22. What is more, it should be noticed that at higher reduced velocity, people may also validate the identified FDs by comparison with the estimations calculated by quasi steady theory [27,68]. This issue should be verified in the future if a wind tunnel, able to generate higher wind speed, is available.

5. Conclusions

This paper illustrates the application of Bayesian spectral density approach on the identification of flutter derivatives, where the buffeting force PSDs can also be obtained. The identification of flutter derivatives is modeled from a probabilistic perspective based on the complex Wishart distribution. Compared with previous time-domain methods (e.g., least square method and stochastic subspace identification technology), the Bayesian spectral density approach is operated in frequency domain, which has advantages over time-domain methods. In uniform flow using free vibration, for example, when the mean wind speed is high, the coupled damping ratio (combined action from structural damping and aerodynamic damping) will increase fast, which means that the free vibration duration is very short. Short free vibration duration can greatly influence the identification accuracy, which is the reason why the identified results at high wind speed are not reliable by least square method. However, with long enough measuring time, the statistical characteristics of buffeting displacement PSDs in frequency domain are stable and reliable. Compared with the stochastic subspace identification technology, the advantage of the frequency-domain Bayesian spectral density approach is that the frequency-domain one does not depend heavily on the assumption that the buffeting force is a white Gaussian process in the broad frequency band (as the case in the stochastic subspace identification). For Bayesian method, we only select a narrow frequency band to infer flutter derivatives, which only demands that the PSD of the buffeting force is constant at that selected narrow band. For Bayesian method, people can also easily incorporate the correlation of buffeting forces in two directions if given a theoretical model of buffeting force's cross spectrum, which is not that easy in the stochastic subspace technology. Because the grids are installed to generate the turbulent flow while conducting the wind tunnel test, the maximum of generated wind speed is relatively lower than that without grids. The advantages of the Bayesian spectral density approach are expected to be more prominent if the mean wind speed is high, which needs to be investigated in the future if a wind tunnel with more wide speed range is available. The identified results in numerical simulations, thin plate model test, and center-slotted girder model test are all satisfactory. In brief, the approach proposed in this paper offers a new angle of view (i.e., probabilistic perspective) for the inference of aerodynamic parameters in wind engineering.

CRediT authorship contribution statement

Xiaolei Chu: Writing – original draft, Conceptualization, Formal analysis, Investigation, Methodology, Validation, Visualization. **Wei Cui:** Conceptualization, Supervision, Writing – review & editing, Funding acquisition. **Peng Liu:** Methodology. **Lin Zhao:** Funding acquisition. **Yaojun Ge:** Supervision, Funding acquisition.

Declaration of competing interest

The authors declare that they have no known competing financial interests or personal relationships that could have appeared to influence the work reported in this paper.

Acknowledgments

The authors appreciate Ph.D. candidates Shengyi Xu, Zilong Wang, and Teng Ma for their assistance in the wind tunnel tests. The authors gratefully acknowledge the support of National Natural Science Foundation of China (52008314, 51978527, 52078383). Any opinions, findings and conclusions are those of the authors and do not necessarily reflect the reviews of the above agencies.

References

- [1] X. Ji, G. Huang, Y.-G. Zhao, Probabilistic flutter analysis of bridge considering aerodynamic and structural parameter uncertainties, *J. Wind Eng. Ind. Aerodyn.* 201 (2020) 104168.
- [2] X. Chu, W. Cui, L. Zhao, S. Cao, Y. Ge, Probabilistic flutter analysis of a long-span bridge in typhoon-prone regions considering climate change and structural deterioration, *J. Wind Eng. Ind. Aerodyn.* 215 (2021) 104701.
- [3] E. Simiu, R.H. Scanlan, *Wind Effects on Structures: Fundamentals and Applications to Design*, John Wiley New York, 1996.
- [4] M. Matsumoto, Aerodynamic damping of prisms, *J. Wind Eng. Ind. Aerodyn.* 59 (2–3) (1996) 159–175.
- [5] B. Siedziako, O. Øiseth, An enhanced identification procedure to determine the rational functions and aerodynamic derivatives of bridge decks, *J. Wind Eng. Ind. Aerodyn.* 176 (2018) 131–142.
- [6] R.H. Scanlan, J. Tomo, Air foil and bridge deck flutter derivatives, *J. Soil Mech. Found. Div* (1971).
- [7] P.P. Sarkar, N.P. Jones, R.H. Scanlan, System identification for estimation of flutter derivatives, *J. Wind Eng. Ind. Aerodyn.* 42 (1–3) (1992) 1243–1254.
- [8] G. Diana, F. Resta, A. Zasso, M. Belloli, D. Rocchi, Forced motion and free motion aeroelastic tests on a new concept dynamometric section model of the Messina suspension bridge, *J. Wind Eng. Ind. Aerodyn.* 92 (6) (2004) 441–462.
- [9] P.P. Sarkar, L. Caracoglia, F.L. Haan Jr., H. Sato, J. Murakoshi, Comparative and sensitivity study of flutter derivatives of selected bridge deck sections, Part 1: Analysis of inter-laboratory experimental data, *Eng. Struct.* 31 (1) (2009) 158–169.
- [10] B. Cao, P.P. Sarkar, Identification of rational functions using two-degree-of-freedom model by forced vibration method, *Eng. Struct.* 43 (2012) 21–30.
- [11] L. Zhao, X. Xie, Y.-y. Zhan, W. Cui, Y.-j. Ge, Z.-c. Xia, S.-q. Xu, M. Zeng, A novel forced motion apparatus with potential applications in structural engineering, *J. Zhejiang Univ. Sci. A* 21 (7) (2020) 593–608.
- [12] B. Siedziako, O. Øiseth, A. Rønquist, An enhanced forced vibration rig for wind tunnel testing of bridge deck section models in arbitrary motion, *J. Wind Eng. Ind. Aerodyn.* 164 (2017) 152–163.
- [13] M. Gu, R. Zhang, H. Xiang, Identification of flutter derivatives of bridge decks, *J. Wind Eng. Ind. Aerodyn.* 84 (2) (2000) 151–162.
- [14] G. Bartoli, S. Contri, C. Mannini, M. Righi, Toward an improvement in the identification of bridge deck flutter derivatives, *J. Eng. Mech.* 135 (8) (2009) 771–785.
- [15] A.G. Chowdhury, P.P. Sarkar, Experimental identification of rational function coefficients for time-domain flutter analysis, *Eng. Struct.* 27 (9) (2005) 1349–1364.
- [16] A. Chen, X. He, H. Xiang, Identification of 18 flutter derivatives of bridge decks, *J. Wind Eng. Ind. Aerodyn.* 90 (12–15) (2002) 2007–2022.
- [17] F. Xu, X. Chen, C. Cai, A. Chen, Determination of 18 flutter derivatives of bridge decks by an improved stochastic search algorithm, *J. Bridge Eng.* 17 (4) (2012) 576–588.
- [18] M. Gu, X.-R. Qin, Direct identification of flutter derivatives and aerodynamic admittances of bridge decks, *Eng. Struct.* 26 (14) (2004) 2161–2172.
- [19] X.-R. Qin, M. Gu, Determination of flutter derivatives by stochastic subspace identification technique, *Wind Struct.* 7 (3) (2004) 173–186.
- [20] T. Janesupasaeree, V. Boonyapinyo, Determination of flutter derivatives of bridge decks by covariance-driven stochastic subspace identification, *Int. J. Struct. Stab. Dyn.* 11 (01) (2011) 73–99.
- [21] S.S. Mishra, K. Kumar, P. Krishna, Identification of 18 flutter derivatives by covariance driven stochastic subspace method, *Wind Struct.* 9 (2) (2006) 159–178.
- [22] V. Boonyapinyo, T. Janesupasaeree, Data-driven stochastic subspace identification of flutter derivatives of bridge decks, *J. Wind Eng. Ind. Aerodyn.* 98 (12) (2010) 784–799.
- [23] Y. Wu, X. Chen, Y. Wang, Identification of linear and nonlinear flutter derivatives of bridge decks by unscented Kalman filter approach from free vibration or stochastic buffeting response, *J. Wind Eng. Ind. Aerodyn.* 214 (2021) 104650.
- [24] D.-W. Seo, L. Caracoglia, Estimation of torsional-flutter probability in flexible bridges considering randomness in flutter derivatives, *Eng. Struct.* 33 (8) (2011) 2284–2296.
- [25] C. Mannini, G. Bartoli, Aerodynamic uncertainty propagation in bridge flutter analysis, *Struct. Saf.* 52 (2015) 29–39.
- [26] S. Au, *Operational Modal Analysis*, Springer, 2017.
- [27] G. Diana, D. Rocchi, T. Argentini, S. Muggiasca, Aerodynamic instability of a bridge deck section model: Linear and nonlinear approach to force modeling, *J. Wind Eng. Ind. Aerodyn.* 98 (6–7) (2010) 363–374.
- [28] J.L. Beck, Bayesian system identification based on probability logic, *Struct. Control Health Monit.* 17 (7) (2010) 825–847.
- [29] Y. Huang, C. Shao, B. Wu, J.L. Beck, H. Li, State-of-the-art review on Bayesian inference in structural system identification and damage assessment, *Adv. Struct. Eng.* 22 (6) (2019) 1329–1351.
- [30] S.-K. Au, Fast Bayesian FFT method for ambient modal identification with separated modes, *J. Eng. Mech.* 137 (3) (2011) 214–226.
- [31] F.-L. Zhang, Y.-C. Ni, S.-K. Au, H.-F. Lam, Fast Bayesian approach for modal identification using free vibration data, Part I—most probable value, *Mech. Syst. Signal Process.* 70 (2016) 209–220.
- [32] Y.-C. Ni, F.-L. Zhang, H.-F. Lam, S.-K. Au, Fast Bayesian approach for modal identification using free vibration data, Part II—Posterior uncertainty and application, *Mech. Syst. Signal Process.* 70 (2016) 221–244.
- [33] S.-K. Au, F.-L. Zhang, Fundamental two-stage formulation for Bayesian system identification, Part I: General theory, *Mech. Syst. Signal Process.* 66 (2016) 31–42.
- [34] F.-L. Zhang, S.-K. Au, Fundamental two-stage formulation for Bayesian system identification, Part II: Application to ambient vibration data, *Mech. Syst. Signal Process.* 66 (2016) 43–61.
- [35] S.-K. Au, F.-L. Zhang, Ambient modal identification of a primary–secondary structure by Fast Bayesian FFT method, *Mech. Syst. Signal Process.* 28 (2012) 280–296.
- [36] H. Sohn, K.H. Law, A Bayesian probabilistic approach for structure damage detection, *Earth. Eng. Struct. Dyn.* 26 (12) (1997) 1259–1281.

- [37] Y. Huang, J.L. Beck, H. Li, Hierarchical sparse Bayesian learning for structural damage detection: theory, computation and application, *Struct. Saf.* 64 (2017) 37–53.
- [38] F.-L. Zhang, C.-W. Kim, Y. Goi, Efficient Bayesian FFT method for damage detection using ambient vibration data with consideration of uncertainty, *Struct. Control Health Monit.* 28 (2) (2021) e2659.
- [39] X. Wang, L. Li, J.L. Beck, Y. Xia, Sparse Bayesian factor analysis for structural damage detection under unknown environmental conditions, *Mech. Syst. Signal Process.* 154 (2021) 107563.
- [40] Y. Wang, K. Huang, Z. Cao, Probabilistic identification of underground soil stratification using cone penetration tests, *Can. Geotech. J.* 50 (7) (2013) 766–776.
- [41] Z.-J. Cao, S. Zheng, D.-Q. Li, K.-K. Phoon, Bayesian identification of soil stratigraphy based on soil behaviour type index, *Can. Geotech. J.* 56 (4) (2019) 570–586.
- [42] K.-V. Yuen, *Bayesian Methods for Structural Dynamics and Civil Engineering*, John Wiley & Sons, 2010.
- [43] N. Goodman, The distribution of the determinant of a complex Wishart distributed matrix, *Ann. Math. Stat.* 34 (1) (1963) 178–180.
- [44] S.-K. Au, Insights on the Bayesian spectral density method for operational modal analysis, *Mech. Syst. Signal Process.* 66 (2016) 1–12.
- [45] H.-F. Lam, J. Hu, J.-H. Yang, Bayesian operational modal analysis and Markov chain Monte Carlo-based model updating of a factory building, *Eng. Struct.* 132 (2017) 314–336.
- [46] O. Sedehi, L.S. Katafygiotis, C. Papadimitriou, Hierarchical Bayesian operational modal analysis: Theory and computations, *Mech. Syst. Signal Process.* 140 (2020) 106663.
- [47] S.H. Cheung, S. Bansal, A new Gibbs sampling based algorithm for Bayesian model updating with incomplete complex modal data, *Mech. Syst. Signal Process.* 92 (2017) 156–172.
- [48] S. Marelli, B. Sudret, UQLab: A framework for uncertainty quantification in Matlab, in: *Vulnerability, Uncertainty, and Risk: Quantification, Mitigation, and Management*, 2014, pp. 2554–2563.
- [49] J. Goodman, J. Weare, Ensemble samplers with affine invariance, *Commun. Appl. Math. Comput. Sci.* 5 (1) (2010) 65–80.
- [50] P. Emil Simiu, P. DongHun Yeo, Wind effects on structures, Wiley Online Library, 1996.
- [51] A. Jain, N.P. Jones, R.H. Scanlan, Coupled flutter and buffeting analysis of long-span bridges, *J. Struct. Eng.* 122 (7) (1996) 716–725.
- [52] A.G. Chowdhury, P.P. Sarkar, A new technique for identification of eighteen flutter derivatives using a three-degree-of-freedom section model, *Eng. Struct.* 25 (14) (2003) 1763–1772.
- [53] L.S. Katafygiotis, K.-V. Yuen, Bayesian spectral density approach for modal updating using ambient data, *Earth. Eng. Struct. Dyn.* 30 (8) (2001) 1103–1123.
- [54] K.-V. Yuen, L.S. Katafygiotis, J.L. Beck, Spectral density estimation of stochastic vector processes, *Probab. Eng. Mech.* 17 (3) (2002) 265–272.
- [55] N.R. Goodman, Statistical analysis based on a certain multivariate complex Gaussian distribution (an introduction), *Ann. Math. Stat.* 34 (1) (1963) 152–177.
- [56] P. Krishnaiah, Some recent developments on complex multivariate distributions, *J. Multivariate Anal.* 6 (1) (1976) 1–30.
- [57] R. Taylor, Interpretation of the correlation coefficient: a basic review, *J. Diagnostic Med. Sonograph.* 6 (1) (1990) 35–39.
- [58] C. Robert, G. Casella, *Monte Carlo Statistical Methods*, Springer Science & Business Media, 2013.
- [59] J.S. Liu, *Monte Carlo Strategies in Scientific Computing*, Springer Science & Business Media, 2008.
- [60] S. Sharma, Markov chain monte carlo methods for bayesian data analysis in astronomy, *Annu. Rev. Astron. Astrophys.* 55 (2017) 213–259.
- [61] E. Simiu, Wind spectra and dynamic alongwind response, *J. Struct. Div.* 100 (9) (1974) 1897–1910.
- [62] H.A. Panofsky, R.A. McCormick, The spectrum of vertical velocity near the surface, *Q. J. R. Meteorol. Soc.* 86 (370) (1960) 495–503.
- [63] M. Shinozuka, C.-M. Jan, Digital simulation of random processes and its applications, *J. Sound Vib.* 25 (1) (1972) 111–128.
- [64] A. Grinsted, Gwmcme: An Implementation of the Goodman and Weare Mcmc Sampler for Matlab, GitHub Repository, 2015.
- [65] S.J. Sheather, M.C. Jones, A reliable data-based bandwidth selection method for kernel density estimation, *J. R. Stat. Soc. Ser. B Stat. Methodol.* 53 (3) (1991) 683–690.
- [66] R.H. Scanlan, Problematics in formulation of wind-force models for bridge decks, *J. Eng. Mech.* 119 (7) (1993) 1353–1375.
- [67] G. Fang, J. Cao, Y. Yang, L. Zhao, S. Cao, Y. Ge, Experimental uncertainty quantification of flutter derivatives for a PK section girder and its application on probabilistic flutter analysis, *J. Bridge Eng.* 25 (7) (2020) 04020034.
- [68] G. Diana, S. Bruni, A. Cigada, A. Collina, Turbulence effect on flutter velocity in long span suspended bridges, *J. Wind Eng. Ind. Aerodyn.* 48 (2–3) (1993) 329–342.